Coordinated Adaptive Robust Contouring Controller Design for an Industrial Biaxial Precision Gantry

Chuxiong Hu, *Student Member, IEEE*, Bin Yao, *Senior Member, IEEE*, and Qingfeng Wang

***Abstract*—To achieve excellent contouring performance, it is no longer possible to neglect dynamic coupling phenomena that occur during contouring controls, especially for a linear-motor-driven industrial biaxial precision gantry, which often moves at high speeds. In addition, effects of significant parametric uncertainties and uncertain nonlinearities need to be addressed carefully. In this paper, a discontinuous-projection-based adaptive robust controller that explicitly takes into account the dynamic coupling effect is developed for the high-performance contouring controls of linear-motor-driven high-speed/acceleration systems under various parametric uncertainties and uncertain nonlinearities. Theoretically, the resulting controllers achieve certain guaranteed transient performance and steady-state tracking accuracy. In addition, asymptotic output tracking is achieved under parametric uncertainties only. Comparative experimental results are obtained for a linear-motor-driven biaxial high-speed industrial gantry. The results verify the excellent contouring performance of the proposed schemes, even in the presence of parametric uncertainties and uncertain nonlinearities.**

***Index Terms*—Adaptive control, contouring, coordinated control, linear motor, task coordinates.**

I. Introduction

As ONE of the most popular solutions to high-speed and high-precision motion applications, linear-motor-driven systems have attracted significant attention and great research efforts during the past decade [1]–[5]. In these designs, each axis of motion is independently driven and the servo controller of each axis receives no information from other axes, which results in a collection of decoupled single-input and single-output controller designs. Decoupled design may be preferable if the disturbance in one axis should not affect the performance of other axes, which is not the real situation in practice. For contouring applications, decoupling could result in the lack of coordination among multiaxes, leading to a degraded contouring performance [6].

Manuscript received February 25, 2009; revised July 7, 2009 and September 7, 2009; accepted September 8, 2009. Date of publication November 17, 2009; date of current version August 4, 2010. Recommended by Technical Editor M. Benbouzid. This work was supported in part by the U.S. National Science Foundation under Grant CMS-0600516 and in part by the National Natural Science Foundation of China under the Joint Research Fund for Overseas Chinese Young Scholars under Grant 50528505.

C. Hu and Q. Wang are with the State Key Laboratory of Fluid Power Transmission and Control, Zhejiang University, Hangzhou 310027, China (e-mail: fyfox.hu@gmail.com; qfwang@zju.edu.cn).

B. Yao is with the School of Mechanical Engineering, Purdue University, West Lafayette, IN 47907 USA, and also with the State Key Laboratory of Fluid Power Transmission and Control, Zhejiang University, Hangzhou 310027, China.

Color versions of one or more of the figures in this paper are available online at http://ieeexplore.ieee.org.

Digital Object Identifier 10.1109/TMECH.2009.2032292

As opposed to the traditional decoupled controls such as [7] and [8], Koren [9] first proposed the cross-coupled control (CCC) strategy that introduced coupling actions in the servo controllers to improve the coordination of axes so that the motion axes are "coordinated" to track the desired contour. Since then, many research publications have been reported on CCC [10]–[12]. However, these designs were based on the classical control theory for linear time-invariant systems, which are applicable only under the assumption that the cross-coupling gains are slowly time-varying. As such, they cannot effectively address the strong dynamic coupling phenomena (e.g., Coriolis force) appearing when tracking curved contours.

During the past decade, contouring control problems have also been approached using different coordination and control strategies. For example, Chiu and Tomizuka [6] formulated the contour tracking problem in a task coordinate frame that is "attached" to the desired contour. Under the task coordinate formulation, a control law can be designed to assign different dynamics to the normal and tangential directions relative to the desired contour. Based on such a task coordinate approach, many specific contouring control schemes have been reported recently [13], [14]. However, all these contouring control techniques did not explicitly address the effect of parametric uncertainties and uncertain nonlinearities. As a result, when stringent contouring performance is of major concern, these methods are often inadequate as actual physical systems are always subjected to certain uncertainties (e.g., the change of payloads).

Yao and coworkers [15]–[18] developed the idea of adaptive robust control (ARC) to provide a rigorous theoretic framework for the precision motion control of systems under both parametric uncertainties and uncertain nonlinearities. The effectiveness of the approach has also been verified through various application studies with comparative experimental results (e.g., [3], [4], and [19]–[21]), in which much improved control performance has been reported.

The objective of this paper is to integrate the recently developed ARC strategy with various coordination strategies using different task coordinate frames to develop practically implementable and yet high-performance contouring controllers for multiaxis high-speed machines. Our earlier endeavor along this line [22] utilizes the concept of generalized curvilinear coordinates introduced in [23] to define the task coordinate frame for coordination. As opposed to the *locally* defined task coordinate frame used in [6], [13], and [14], which depends on the desired motion trajectory as well, the general task space defined by a set of curvilinear coordinates in [23] could be globally defined based on the shape of the desired contour only, and thus, has nothing to do with the specific desired motions to be tracked on

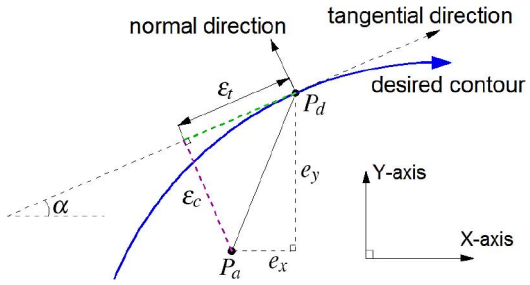

Fig. 1. Approximate contouring error model.

the contour. However, such a formulation of task space does not guarantee the orthogonality of the generalized coordinates. As such, only circular contour experiments were performed in [22] as the resulting generalized curvilinear coordinates happened to be orthogonal along the desired circular contour. To solve this issue and provide an equal platform for comparing various coordinated contouring controllers, this paper will use the same task coordinate frame as used by other researchers [6], [13], [14]. Though locally defined based on the desired contour and the desired motion trajectories, such a task coordinate frame always ensures the local orthogonality of task coordinates, and thus, can be used for noncircular contouring experiments as well. With such a task coordinate frame for coordination, the discontinuous-projection-based ARC design [15], [24] is used to construct coordinated contouring controllers, which explicitly take into account the effect of various parametric uncertainties and uncertain nonlinearities for a much improved contouring performance. Comparative experimental results obtained on a high-speed Anorad industrial biaxial gantry with a linear encoder resolution of 0.5 μm will be presented to illustrate the much improved contouring performance of the proposed controllers despite various model uncertainties.

II. Problem Formulation

A. Task Coordinate Frame

By definition, contouring error represents the geometric deviation from the actual contour to the desired contour, and hence, it can be quantitatively defined as the minimum distance from the actual position to the desired contour. However, accurate calculation of contouring error often leads to an intensive computation task, which is hard to be realized in practice, and this definition is often replaced by approximate models for the contour tracking purposes [14].

A popular approximation of contouring error is presented in [11] and [14], as shown in Fig. 1. Let x and y denote the horizontal and the vertical axes of a biaxial gantry system, respectively. Let P_d and P_a denote the position of the reference command and the actual position of the system at any time instant, respectively. At point P_d, the desired contour possesses a set of tangential and normal directions such that the contouring error can be approximated by the distance from P_a to the tangential line in the normal direction. By this definition, the contouring error ε_c can be approximately computed by the normal error ε_n as

$$\varepsilon_c \approx \varepsilon_n = -\sin\alpha e_x + \cos\alpha e_y \tag{1}$$

where e_x and e_y denote the axial tracking errors of x and y axes, i.e., $e_x = x - x_d$ and $e_y = y - y_d$, and α denotes the angle between the tangential line and the horizontal *X*-axis. In this model, if the axial tracking errors are comparatively less than the curvature of the desired contour, then it yields a good approximation of the contouring error.

However, the tangential error ε_t can be described as

$$\varepsilon_t = \cos\alpha e_x + \sin\alpha e_y. \tag{2}$$

Then, the tangential and the normal directions are mutually orthogonal, and hence, can be taken as the new basis for the task coordinate frame. Thus, the physical (x, y) coordinates can be transformed into the task $(\varepsilon_c, \varepsilon_t)$ coordinates by a linear time-varying transformation

$$\varepsilon = \mathbf{T}\mathbf{e} \tag{3}$$

where $\varepsilon = [\varepsilon_c, \varepsilon_t]^T$, $\mathbf{e} = [e_x, e_y]^T$, and the time-varying transformation matrix depends on the reference trajectories for the desired contour only and is given by

$$\mathbf{T} = \begin{bmatrix} -\sin\alpha & \cos\alpha \\ \cos\alpha & \sin\alpha \end{bmatrix}. \tag{4}$$

The matrix $\mathbf{T}$ is always unitary for all values of α, i.e., $\mathbf{T}^T = \mathbf{T}$ and $\mathbf{T}^{-1} = \mathbf{T}$.

B. System Dynamics

The biaxial linear-motor-driven gantry is assumed to have the following dynamics [19]:

$$\mathbf{M}\ddot{\mathbf{q}} + \mathbf{B}\dot{\mathbf{q}} + \mathbf{F}(\dot{\mathbf{q}}) = \mathbf{u} + \mathbf{d} \tag{5}$$

where $\mathbf{q} = [x(t), y(t)]^T$, $\dot{\mathbf{q}} = [\dot{x}(t), \dot{y}(t)]^T$, and $\ddot{\mathbf{q}} = [\ddot{x}(t), \ddot{y}(t)]^T$ are the 2×1 vectors of the axis position, velocity, and acceleration, respectively; $\mathbf{u}$ is the 2×1 vector of control input; $\mathbf{d}$ is the 2×1 vector of unknown nonlinear functions, including external disturbances and other unmodeled forces such as the cogging forces of linear motors; $\mathbf{M} = \text{diag}[M_1, M_2]$ and $\mathbf{B} = \text{diag}[B_1, B_2]$ are the 2×2 diagonal inertia and damping matrices, respectively; and $\mathbf{F}(\dot{\mathbf{q}})$ is the 2×1 vector of nonlinear friction, i.e., $\mathbf{F}(\dot{\mathbf{q}}) = [F_1(\dot{x}), F_2(\dot{y})]^T$, and F_i, $i = 1, 2$, is approximated by a simple smooth friction model given by $\bar{\mathbf{F}}(\dot{\mathbf{q}}) = \mathbf{A}\mathbf{S}_\mathbf{f}(\dot{\mathbf{q}})$, where $\mathbf{A} = \text{diag}[A_1, A_2]$ is the 2×2 diagonal friction coefficient matrix and $\mathbf{S}_\mathbf{f}(\cdot)$ is a vector-valued smooth function, i.e., $\mathbf{S}_\mathbf{f}(\dot{\mathbf{q}}) = [S_f(\dot{x}), S_f(\dot{y})]^T$. Define the friction model approximation error as $\tilde{\mathbf{F}} = \bar{\mathbf{F}} - \mathbf{F}$. Then, (5) can be written as

$$\mathbf{M}\ddot{\mathbf{q}} + \mathbf{B}\dot{\mathbf{q}} + \mathbf{A}\mathbf{S}_\mathbf{f}(\dot{\mathbf{q}}) = \mathbf{u} + \mathbf{d}_\mathbf{n} + \tilde{\mathbf{d}} \tag{6}$$

where $\mathbf{d}_\mathbf{n} = [d_{n1}, d_{n2}]^T$ is the nominal value of $\mathbf{d}_1 = \mathbf{d} + \tilde{\mathbf{F}}$ and $\tilde{\mathbf{d}} = \mathbf{d}_1 - \mathbf{d}_\mathbf{n}$. For this dynamic system, we define the tracking error as $\mathbf{e} = [e_x, e_y]^T = [x(t) - x_d(t), y(t) - y_d(t)]^T$, where $\mathbf{q_d}(t) = [x_d(t), y_d(t)]^T$ is given to describe the desired contour. Then, the system dynamics can be rewritten as

$$\mathbf{M}\ddot{\mathbf{e}} + \mathbf{B}\dot{\mathbf{e}} + \mathbf{A}\mathbf{S}_\mathbf{f}(\dot{\mathbf{q}}) + \mathbf{M}\ddot{\mathbf{q}}_\mathbf{d} + \mathbf{B}\dot{\mathbf{q}}_\mathbf{d} = \mathbf{u} + \mathbf{d}_\mathbf{n} + \tilde{\mathbf{d}}. \tag{7}$$

Noting (3) and (4), and the unitary property of $\mathbf{T}$, the time derivatives of the tracking error states can be derived as [14]

$$\dot{\mathbf{e}} = \mathbf{T}\dot{\varepsilon} + \dot{\mathbf{T}}\varepsilon \qquad \ddot{\mathbf{e}} = \mathbf{T}\ddot{\varepsilon} + \mathbf{2}\dot{\mathbf{T}}\dot{\varepsilon} + \ddot{\mathbf{T}}\varepsilon. \tag{8}$$

Then, the system dynamics can be represented in the task coordinate frame as

$$\mathbf{M_t}\ddot{\varepsilon} + \mathbf{B_t}\dot{\varepsilon} + 2\mathbf{C_t}\dot{\varepsilon} + \mathbf{D_t}\varepsilon + \mathbf{M_q}\ddot{\mathbf{q}}_\mathbf{d} + \mathbf{B_q}\dot{\mathbf{q}}_\mathbf{d} + \mathbf{A_q}\mathbf{S_f}(\dot{\mathbf{q}}) = \mathbf{u_t} + \mathbf{d_t} + \widetilde{\Delta} \tag{9}$$

where

$$\begin{aligned} &\mathbf{M_t} = \mathbf{TMT}, \quad \mathbf{B_t} = \mathbf{TBT}, \quad \mathbf{C_t} = \mathbf{TM}\dot{\mathbf{T}} \\ &\mathbf{D_t} = \mathbf{TM}\ddot{\mathbf{T}} + \mathbf{TB}\dot{\mathbf{T}}, \quad \mathbf{u_t} = \mathbf{Tu}, \quad \mathbf{d_t} = \mathbf{Td_n}, \quad \widetilde{\Delta} = \mathbf{T}\widetilde{\mathbf{d}} \\ &\mathbf{M_q} = \mathbf{TM}, \quad \mathbf{B_q} = \mathbf{TB}, \quad \mathbf{A_q} = \mathbf{TA}. \end{aligned} \tag{10}$$

It is well known that (9) has several properties [25].

P1) In any finite work space $\mathbf{q} \in \Omega_\mathbf{q}$, $\mathbf{M_t}$ is a symmetric positive-definite (s.p.d.) matrix with

$$\mu_1 \mathbf{I} \le \mathbf{M_t} \le \mu_2 \mathbf{I} \qquad \forall \mathbf{q} \in \Omega_\mathbf{q} \tag{11}$$

where μ_1 and μ_2 are two positive scalars.

P2) Given the definitions in (10), the matrix $\mathbf{N} = \dot{\mathbf{M}}_\mathbf{t} - \mathbf{2C_t}$ is a skew-symmetric matrix.

P3) The matrices or vectors in (9), $\mathbf{M_t}, \mathbf{B_t}, \mathbf{C_t}, \mathbf{D_t}, \mathbf{M_q}, \mathbf{B_q}, \mathbf{A_q}$, and $\mathbf{d_t}$, can be linearly parameterized by a set of parameters defined by $\theta = [\theta_1, \ldots, \theta_8]^T = [M_1, M_2, B_1, B_2, A_1, A_2, d_{n1}, d_{n2}]^T$.

In general, the parameter θ cannot be known exactly. For example, the payload of the biaxial gantry depends on tasks. However, the extent of parametric uncertainties can be predicted. Therefore, the following practical assumption is made.[1]

Assumption 1: The extent of the parametric uncertainties and uncertain nonlinearities is known, i.e.,

$$\theta \in \Omega_\theta \triangleq \{\theta : \ \theta_{\min} \le \theta \le \theta_{\max}\} \tag{12}$$

$$\widetilde{\Delta} \in \Omega_\Delta \triangleq \{\widetilde{\Delta} : \ \|\widetilde{\Delta}\| \le \delta_\Delta\} \tag{13}$$

where $\theta_{\min} = [\theta_{1\min}, \ldots, \theta_{8\min}]^T$ and $\theta_{\max} = [\theta_{1\max}, \ldots, \theta_{8\max}]^T$ are known, and δ_Δ is a known function.

The control objective is to synthesize a control input $\mathbf{u_t}$ such that $\mathbf{q} = [x, y]^T$ tracks the reference trajectory $\mathbf{q_d}(t) = [x_d, y_d]^T$ describing the desired contour. $\mathbf{q_d}(t)$ is assumed to be of at least second-order differentiable.

III. Discontinuous Projection

Let $\widehat{\theta}$ denote the estimate of θ and $\widetilde{\theta}$ denote the estimation error (i.e., $\widetilde{\theta} = \widehat{\theta} - \theta$). In view of (12), the following adaptation law with discontinuous projection modification can be used:

$$\dot{\widehat{\theta}} = \mathrm{Proj}_{\widehat{\theta}}(\Gamma\tau) \tag{14}$$

[1]For simplicity, the following notations are used: $\bullet_i$ for the ith component of the vector $\bullet$, $\bullet_{\min}$ for the minimum value of $\bullet$, and $\bullet_{\max}$ for the maximum value of $\bullet$. The operation $\le$ for two vectors is performed in terms of the corresponding elements of the vectors.

where $\Gamma > 0$ is a diagonal matrix and τ is an adaptation function to be synthesized later. The projection mapping $\mathrm{Proj}_{\widehat{\theta}}(\bullet) = [\mathrm{Proj}_{\widehat{\theta}_1}(\bullet_1), \ldots, \mathrm{Proj}_{\widehat{\theta}_8}(\bullet_8)]^T$ is defined in [15] as

$$\mathrm{Proj}_{\widehat{\theta}_i}(\bullet_i) = \begin{cases} 0, & \text{if } \widehat{\theta}_i = \theta_{i\max} \text{ and } \bullet_i > 0 \\ 0, & \text{if } \widehat{\theta}_i = \theta_{i\min} \text{ and } \bullet_i < 0 \\ \bullet_i, & \text{otherwise.} \end{cases} \tag{15}$$

It can be shown that for any adaptation function τ, the projection mapping used in (15) guarantees the following [16]:

P4)

$$\widehat{\theta} \in \Omega_\theta \triangleq \{\widehat{\theta} : \theta_{i\min} \le \widehat{\theta} \le \theta_{i\max}\} \tag{16}$$

P5)

$$\widetilde{\theta}^T(\Gamma^{-1}\mathrm{Proj}_{\widehat{\theta}}(\Gamma\tau) - \tau) \le 0 \qquad \forall\tau. \tag{17}$$

IV. ARC Law Synthesis

The task space dynamics (9) have the same form as those in [22]. Thus, the same controller design procedure and the proof of theoretical performance as in [22] can be applied. Therefore, in the following, only the design of controllers and the theoretically achievable results of each controller are given with all proofs omitted. Specifically, define a switching-function-like quantity as

$$\mathbf{s} = \dot{\varepsilon} + \Lambda\varepsilon \tag{18}$$

where $\Lambda > 0$ is a diagonal matrix. Define a positive-semidefinite (p.s.d.) function

$$V(t) = \frac{\mathbf{1}}{\mathbf{2}}\mathbf{s^T}\mathbf{M_t}\mathbf{s}. \tag{19}$$

Differentiating V yields

$$\dot{V} = \mathbf{s^T}[\mathbf{u_t} + \mathbf{d_t} + \widetilde{\Delta} - \mathbf{M_q}\ddot{\mathbf{q}}_\mathbf{d} - \mathbf{B_q}\dot{\mathbf{q}}_\mathbf{d} - \mathbf{A_q}\mathbf{S_f}(\dot{\mathbf{q}}) - \mathbf{B_t}\dot{\varepsilon} - \mathbf{C_t}\dot{\varepsilon} - \mathbf{D_t}\varepsilon + \mathbf{C_t}\Lambda\varepsilon + \mathbf{M_t}\Lambda\dot{\varepsilon}] \tag{20}$$

where P2) is used to eliminate the term $(\mathbf{1/2})\mathbf{s^T}\dot{\mathbf{M}}_\mathbf{t}\mathbf{s}$. Furthermore, from P3), we can linearly parameterize the terms in (20) as

$$\mathbf{M_q}\ddot{\mathbf{q}}_\mathbf{d} + \mathbf{B_q}\dot{\mathbf{q}}_\mathbf{d} + \mathbf{A_q}\mathbf{S_f}(\dot{\mathbf{q}}) + \mathbf{B_t}\dot{\varepsilon} + \mathbf{C_t}\dot{\varepsilon} + \mathbf{D_t}\varepsilon - \mathbf{C_t}\Lambda\varepsilon - \mathbf{M_t}\Lambda\dot{\varepsilon} - \mathbf{d_t} = -\Psi(\mathbf{q}, \dot{\mathbf{q}}, t)\theta \tag{21}$$

where Ψ is a 2×8 matrix of known functions, known as the regressor. Equation (20) can thus be rewritten as

$$\dot{V} = \mathbf{s^T}[\mathbf{u_t} + \Psi(\mathbf{q}, \dot{\mathbf{q}}, t)\theta + \widetilde{\Delta}]. \tag{22}$$

Noting the structure of (22), the following ARC law is proposed:

$$\mathbf{u_t} = \mathbf{u_a} + \mathbf{u_s}, \qquad \mathbf{u_a} = -\Psi(\mathbf{q}, \dot{\mathbf{q}}, t)\widehat{\theta} \tag{23}$$

where $\mathbf{u_a}$ is the adjustable model compensation needed to achieve perfect tracking and $\mathbf{u_s}$ is a robust control law to be synthesized later. Substituting (23) into (22) and simplifying the resulting expression lead to

$$\dot{V} = \mathbf{s^T}[\mathbf{u_s} - \Psi(\mathbf{q}, \dot{\mathbf{q}}, t)\widetilde{\theta} + \widetilde{\Delta}]. \tag{24}$$

The robust control function $\mathbf{u_s}$ consists of two terms

$$\mathbf{u_s} = \mathbf{u_{s1}} + \mathbf{u_{s2}}, \qquad \mathbf{u_{s1}} = -\mathbf{K}\mathbf{s} \tag{25}$$

where $\mathbf{u_{s1}}$ is used to stabilize the nominal system, which is chosen to be a simple proportional feedback with $\mathbf{K}$ being an s.p.d. matrix for simplicity, and $\mathbf{u_{s2}}$ is a feedback used to attenuate the effect of model uncertainties for a guaranteed robust performance. Noting Assumption 1 and (16) of P4), there exists a $\mathbf{u_{s2}}$ such that the following two conditions are satisfied [15]:

$$\begin{aligned} &1) \qquad \mathbf{s^T}\{\mathbf{u_{s2}} - \Psi(\mathbf{q}, \dot{\mathbf{q}}, t)\widetilde{\theta} + \widetilde{\Delta}\} \le \eta \\ &2) \qquad \mathbf{s^T}\mathbf{u_{s2}} \le \mathbf{0} \end{aligned} \tag{26}$$

where η is a design parameter that can be arbitrarily small. One smooth example of $\mathbf{u_{s2}}$ satisfying (26) is given by $\mathbf{u_{s2}} = -(\mathbf{1}/\mathbf{4}\eta)h^2\mathbf{s}$, where h is any smooth function satisfying $h \ge \|\theta_{\mathbf{M}}\|\|\Psi(\mathbf{q}, \dot{\mathbf{q}}, t)\| + \delta_\Delta$, and $\theta_M = \theta_{\max} - \theta_{\min}$.

Theorem 1: Suppose the adaptation function in (14) is chosen as

$$\tau = \Psi^{\mathbf{T}}(\mathbf{q}, \dot{\mathbf{q}}, t)\mathbf{s}. \tag{27}$$

Then, the ARC control law (23) guarantees the following.

1) In general, all signals are bounded. Furthermore, the p.s.d. function $V(t)$ defined by (19) is bounded above by

$$V(t) \le \exp(-\lambda t)V(0) + \frac{\eta}{\lambda}\left[1 - \exp(-\lambda t)\right] \tag{28}$$

where $\lambda = 2\sigma_{\min}(\mathbf{K})/\mu_2$ and $\sigma_{\min}(\cdot)$ denotes the minimum eigenvalue of a matrix.

2) Suppose after a finite time t_0, there exist parametric uncertainties only, i.e., $\widetilde{\Delta} = 0\ \forall t \ge t_0$. Then, in addition to result 1), zero final tracking error is also achieved, i.e., $\mathbf{e} \to 0$ and $\mathbf{s} \to 0$ as $t \to \infty$.

V. Desired Compensation ARC

In the ARC design presented in Section IV, the regressor $\Psi(\mathbf{q}, \dot{\mathbf{q}}, t)$ in the model compensation $\mathbf{u_a}$ (23) and the adaptation function τ (27) depend on states $\mathbf{q}$ and $\dot{\mathbf{q}}$, respectively. Such an adaptation structure may have several potential implementation problems [26]. First, the effect of measurement noise may be severe, and a slow adaptation rate may have to be used, which, in turn, reduces the effect of parameter adaptation. Second, there may exist certain interactions between the model compensation $\mathbf{u_a}$ and the robust control $\mathbf{u_s}$. This may complicate the controller gain tuning process in implementation. Sadegh and Horowitz [27] proposed a desired compensation adaptation law in which the regressor is calculated only by the desired trajectory information. This idea was then incorporated in the ARC design in [24] and [26]. In the following, the desired compensation ARC (DCARC) is applied on the biaxial linear-motor-driven gantry as well.

The proposed DCARC law and adaptation function have the same form as (23) and (27), but with the regressor $\Psi(\mathbf{q}, \dot{\mathbf{q}}, t)$ substituted by the desired regressor $\Psi_{\mathbf{d}}(\mathbf{q_d}(t), \dot{\mathbf{q}}_{\mathbf{d}}(t), t)$

$$\mathbf{u_t} = \mathbf{u_a} + \mathbf{u_s}, \qquad \mathbf{u_a} = -\Psi_{\mathbf{d}}\widehat{\theta}, \qquad \tau = \Psi_{\mathbf{d}}^{\mathbf{T}}\mathbf{s}. \tag{29}$$

Choose a p.s.d function

$$V(t) = \frac{\mathbf{1}}{\mathbf{2}}\mathbf{s^T}\mathbf{M_t}\mathbf{s} + \frac{\mathbf{1}}{\mathbf{2}}\varepsilon^{\mathbf{T}}\mathbf{K}_\varepsilon\varepsilon \tag{30}$$

where $\mathbf{K}_\varepsilon$ is a diagonal positive-definite matrix. Differentiating $V(t)$ and substituting (29) into the resulting expression yields

$$\dot{V} = \mathbf{s^T}[\mathbf{u_s} + \widetilde{\Psi}\theta - \Psi_{\mathbf{d}}\widetilde{\theta} + \widetilde{\Delta}] + \varepsilon^T\mathbf{K}_\varepsilon\dot{\varepsilon} \tag{31}$$

where $\widetilde{\Psi} = \Psi(\mathbf{q}, \dot{\mathbf{q}}, t) - \Psi_{\mathbf{d}}(\mathbf{q_d}, \dot{\mathbf{q}}_{\mathbf{d}}, t)$ is the difference between the actual regression matrix and the desired regression matrix formulations. As shown in [27], $\widetilde{\Psi}$ can be quantified as

$$\|\widetilde{\Psi}\theta\| \le \zeta_1\|\varepsilon\| + \zeta_2\|\varepsilon\|^2 + \zeta_3\|\mathbf{s}\| + \zeta_4\|\mathbf{s}\|\|\varepsilon\| \tag{32}$$

where $\zeta_1, \zeta_2, \zeta_3$, and ζ_4 are positive bounding constants that depend on the desired contour and the physical properties of the biaxial gantry. Similar to (25), the robust control function $\mathbf{u_s}$ consists of two terms given by

$$\mathbf{u_s} = \mathbf{u_{s1}} + \mathbf{u_{s2}}, \qquad \mathbf{u_{s1}} = -\mathbf{K}\mathbf{s} - \mathbf{K}_\varepsilon\varepsilon - \mathbf{K_a}\|\varepsilon\|^2\mathbf{s} \tag{33}$$

where the controller parameters $\mathbf{K}$, $\mathbf{K}_\varepsilon$, and $\mathbf{K_a}$ are s.p.d. matrices satisfying $\sigma_{\min}(\mathbf{K_a}) \ge \zeta_2 + \zeta_4$ and the following condition:

$$\mathbf{Q} = \begin{bmatrix} \sigma_{\min}(\mathbf{K}_\varepsilon\Lambda) - \dfrac{1}{4}\zeta_2 & -\dfrac{1}{2}\zeta_1 \\ -\dfrac{1}{2}\zeta_1 & \sigma_{\min}(\mathbf{K}) - \zeta_3 - \dfrac{1}{4}\zeta_4 \end{bmatrix} > 0. \tag{34}$$

Specifically, it is easy to check that if

$$\sigma_{\min}(\mathbf{K}_\varepsilon\Lambda) \ge \frac{1}{2}\zeta_1 + \frac{1}{4}\zeta_2 \qquad \sigma_{\min}(\mathbf{K}) \ge \frac{1}{2}\zeta_1 + \zeta_3 + \frac{1}{4}\zeta_4 \tag{35}$$

the matrix $\mathbf{Q}$ defined in (34) is positive-definite. The robust control term $\mathbf{u_{s2}}$ is required to satisfy the following constrains similar to (26):

$$\begin{aligned} &1) \qquad \mathbf{s^T}\{\mathbf{u_{s2}} - \Psi_{\mathbf{d}}\widetilde{\theta} + \widetilde{\Delta}\} \le \eta \\ &2) \qquad \mathbf{s^T}\mathbf{u_{s2}} \le \mathbf{0}. \end{aligned} \tag{36}$$

One smooth example of $\mathbf{u_{s2}}$ satisfying (36) is $\mathbf{u_{s2}} = -(1/4\eta)h_d^2\mathbf{s}$, where h_d is any function satisfying $h_d \ge \|\theta_{\mathbf{M}}\|\|\Psi_{\mathbf{d}}\| + \delta_\Delta$.

Theorem 2: The DCARC law (29) guarantees the following.

1) In general, all signals are bounded. Furthermore, the p.s.d. function $V(t)$ defined by (30) is bounded above by

$$V(t) \le \exp(-\lambda t)V(0) + \frac{\eta}{\lambda}\left[1 - \exp(-\lambda t)\right] \tag{37}$$

where $\lambda = 2\sigma_{\min}(\mathbf{Q})/(\max[\mu_2, \sigma_{\max}(\mathbf{K}_\varepsilon)])$, and $\sigma_{\max}(\cdot)$ denotes the maximum eigenvalue of a matrix.

2) Suppose after a finite time t_0, there exist parametric uncertainties only, i.e., $\widetilde{\Delta} = 0\ \forall t \ge t_0$. Then, in addition to result 1), zero final tracking error is also achieved, i.e., $\varepsilon \to 0$ and $\mathbf{s} \to 0$ as $t \to \infty$.

VI. Experimental Setup and Results

A. Experimental Setup

To study contour-following motion control and test the proposed controllers' effectiveness in practical implementation, a

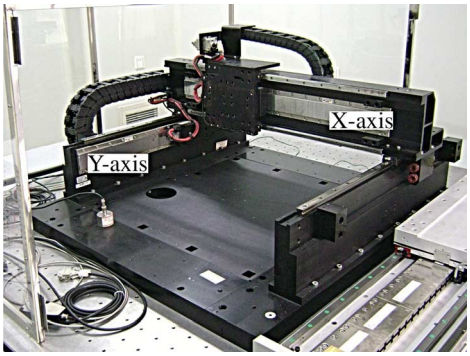

Fig. 2. Biaxial linear-motor-driven gantry system.

biaxial Anorad HERC-510-510-AA1-B-CC2 gantry from Rockwell Automation is set up at Zhejiang University as a test bed. As shown in Fig. 2, the two axes of the gantry are mounted orthogonally with *X*-axis on top of *Y*-axis. The position sensors of the gantry are two linear encoders with a resolution of 0.5 μm after quadrature. The velocity signal is obtained by the difference of two consecutive position measurements. Standard least-square identification is performed to obtain the parameters of the biaxial gantry, and it is found that nominal values of the gantry system parameters without loads are $\theta = [0.115, 0.5, 0.26, 0.4, 0.1, 0.15, 0, 0]^T$. The bounds of the parametric variations are chosen as

$$\theta_{\min} = [0.06, 0.5, 0.15, 0.1, 0.05, 0.08, -0.5, -1]^T$$
$$\theta_{\max} = [0.20, 0.75, 0.35, 0.5, 0.15, 0.5, 0.5, 1]^T. \quad (38)$$

B. Performance Indexes

As in [19], the following performance indexes will be used to measure the quality of each control algorithm [19].

1) $\|\varepsilon_c\|_{\rm rms} = ((1/T)\int_0^T |\varepsilon_c|^2 dt)^{1/2}$, the rms value of the contouring error, is used to measure average contouring performance, where T represents the total running time.
2) $\varepsilon_{cM} = \max_t\{|\varepsilon_c|\}$, the maximum absolute value of the contouring error, is used to measure transient performance.
3) $\|u_i\|_{\rm rms} = ((1/T)\int_0^T |u_i|^2 dt)^{1/2}$, the average control input of each axis, is used to evaluate the amount of control effort.

C. Experimental Results

The control algorithms are implemented using a dSPACE DS1103 controller board. The controller executes programs at a sampling period of $T_s = 0.2$ ms, resulting in a velocity measurement resolution of 0.0025 m/s. The following control algorithms are compared.

C1) *Proportional–integral–differential (PID) controllers for each axis separately:* The control parameters are set as K_p, K_i, and K_d. For *X*-axis, $K_p = 18\,000$, $K_i = 300\,000$, and $K_d = 65$; for *Y*-axis, $K_p = 15\,000$, $K_i = 140\,000$, and $K_d = 120$. These PID gains are chosen so that the resulting nominal closed-loop transfer functions have a pair of dominant poles with break frequencies of 383 and 166 rad/s and damping ratios around 0.7 for *X*-axis and *Y*-axis, respectively; the third closed-loop poles are around -17.78 and -10.124 for *X*-axis and *Y*-axis, respectively, but their effects are pretty much canceled by the nearby zeros at -17.81 and -10.15.

C2) *ARC—The control law proposed in Section IV:* The smooth functions $S_f(\dot{x})$ and $S_f(\dot{y})$ are chosen as $2/\pi \arctan(9000\dot{x})$ and $2/\pi \arctan(9000\dot{y})$. The design parameter Λ is chosen as $\Lambda = \text{diag}[100, 30]$. $\mathbf{u_{s2}}$ in (25) is given in Section IV. Theoretically, we should use the form $\mathbf{u_{s2}} = -\mathbf{K_{s2}}(\mathbf{q})\mathbf{s}$, with $\mathbf{K_{s2}}(\mathbf{q})$ being a nonlinear proportional feedback gain as given in [17] to satisfy the robust performance requirement (26) globally. In implementation, a large enough constant feedback gain $\mathbf{K_{s2}}$ is used instead to simplify the resulting control law. With such a simplification, though the robust performance condition (26) may not be guaranteed globally, the condition can still be satisfied in a large enough working range that might be acceptable to practical applications, as done in [20]. With this simplification, noting (25), we choose $\mathbf{u_s} = -\mathbf{K_s}\mathbf{s}$ in the experiments, where $\mathbf{K_s}$ represents the summation of $\mathbf{K}$ and $\mathbf{K_{s2}}$ and is chosen as $\mathbf{K_s} = \text{diag}[100, 60]$. The adaptation rates are set as $\Gamma = \text{diag}[10, 10, 10, 10, 1, 1, 10\,000, 10\,000]$. The initial parameter estimates are chosen as $\widehat{\theta}(0) = [0.1, 0.55, 0.20, 0.22, 0.1, 0.15, 0, 0]$.

C3) *DCARC—The control law proposed in Section V:* The smooth functions $S_f(\dot{x}_d)$ and $S_f(\dot{y}_d)$ are chosen as $2/\pi \arctan(9000\dot{x}_d)$ and $2/\pi \arctan(9000\dot{y}_d)$, respectively. The design parameters Λ is chosen as $\Lambda = \text{diag}[100, 30]$. Similar to that in C2), we choose $\mathbf{u_s} = -\mathbf{K_s}\mathbf{s} - \mathbf{K}_\varepsilon\varepsilon - \mathbf{K_a}\|\varepsilon\|^2\mathbf{s}$ in the experiments instead of (33), where $\mathbf{K_s}$ represents the combined gain of $\mathbf{u_{s1}}$ and $\mathbf{u_{s2}}$, and the controller parameters are chosen as $\mathbf{K_s} = \text{diag}[100, 60]$, $\mathbf{K_a} = \text{diag}[10\,000, 10\,000]$, and $\mathbf{K_e} = \text{diag}[5000, 5000]$. The adaptation rates are set as $\Gamma = \text{diag}[10, 10, 10, 10, 1, 1, 10\,000, 10\,000]$. For comparison purpose, the same initial conditions as those in ARC are used.

The following test sets are performed.

Set 1: To test the nominal contouring performance of the controllers, experiments are run without payload.

Set 3: To test the performance robustness of the algorithms to parameter variations, a 5.2-kg payload is mounted on the gantry.

Set 3: A large step disturbance (a simulated 0.6-V electrical signal) is added to the input of *Y*-axis at $t = 1.86$ s and removed at $t = 4.86$ s to test the performance robustness of each controller to disturbance.

1) Circular Contouring With Constant Velocity: To test the contouring performance of the proposed algorithms, the biaxial gantry is first commanded to track a circle given by

$$\mathbf{q_d} = \begin{bmatrix} x_d(t) \\ y_d(t) \end{bmatrix} = \begin{bmatrix} 0.2\sin(2t) \\ -0.2\cos(2t) + 0.2 \end{bmatrix} \quad (39)$$

which has a desired velocity of $v = 0.4$ m/s on the contour.

The circular contouring experimental results in terms of performance indexes after running the gantry for one period are given in Table I. As seen from the table, both ARC and DCARC achieve better steady-state contouring performance during fast circular movements than PID. Overall, DCARC performs better

TABLE I
CIRCULAR CONTOURING RESULTS

	$\|\|\varepsilon_c\|\|_{rms}$	ε_{cM}	$\|\|\varepsilon_l\|\|_{rms}$	$\|\|u_x\|\|_{rms}$	$\|\|u_y\|\|_{rms}$
C1 (Set1)	$6.42\mu m$	$25.53\mu m$	$6.00\mu m$	0.24V	0.44V
C2 (Set1)	$1.95\mu m$	$6.86\mu m$	$6.59\mu m$	0.29V	0.48V
C3 (Set1)	$1.77\mu m$	$6.33\mu m$	$4.63\mu m$	0.30V	0.50V
C1 (Set2)	$6.59\mu m$	$25.77\mu m$	$6.40\mu m$	0.25V	0.47V
C2 (Set2)	$2.13\mu m$	$8.55\mu m$	$6.83\mu m$	0.30V	0.51V
C3 (Set2)	$1.87\mu m$	$7.29\mu m$	$5.88\mu m$	0.32V	0.51V
C1 (Set3)	$6.89\mu m$	$44.35\mu m$	$6.22\mu m$	0.24V	0.44V
C2 (Set3)	$2.34\mu m$	$26.89\mu m$	$6.77\mu m$	0.29V	0.48V
C3 (Set3)	$2.06\mu m$	$23.28\mu m$	$4.79\mu m$	0.30V	0.49V

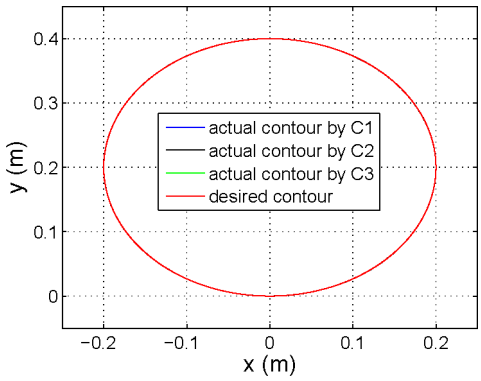

Fig. 3. Circular contouring of set 1 in X–Y plane.

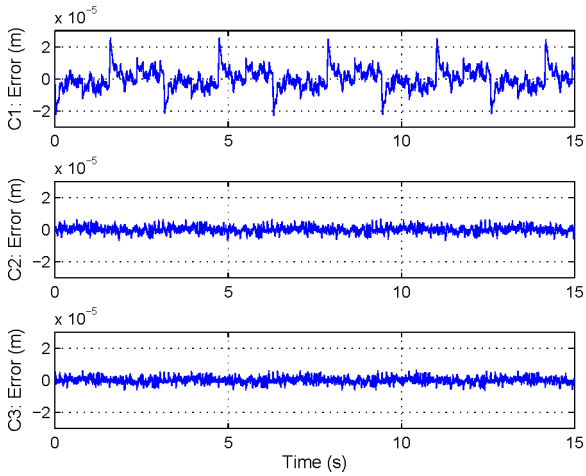

Fig. 4. Circular contouring errors of set 1 (no load).

than ARC in terms of all indexes. It can also be observed that, as expected, all controllers use almost the same amount of control efforts for every test set. For set 1, the desired circle and the actual contours by all three controllers are shown in Fig. 3, and the contouring errors are given in Fig. 4, demonstrating the good nominal performance of both ARC and DCARC controllers—the contouring errors are mostly within 5 μm. For set 2, the contouring errors are displayed in Fig. 5, which shows that both ARC and DCARC achieve almost the same good steady-state contouring performance as before despite the change of inertia load, thus verifying the performance robustness of the proposed ARC controllers to parameter variations. The contouring errors of set 3 are given in Fig. 6. As seen from the figures, the added

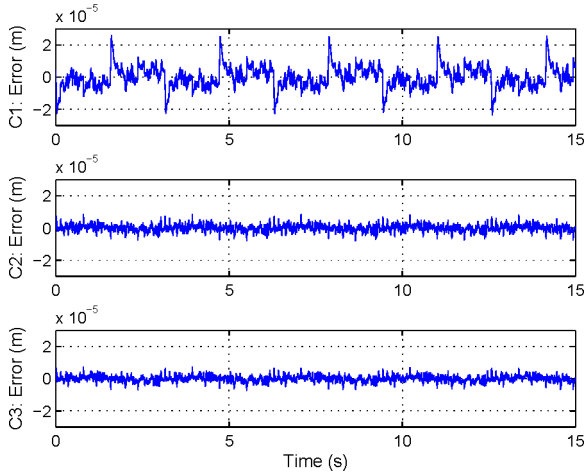

Fig. 5. Circular contouring errors of set 2 (loaded).

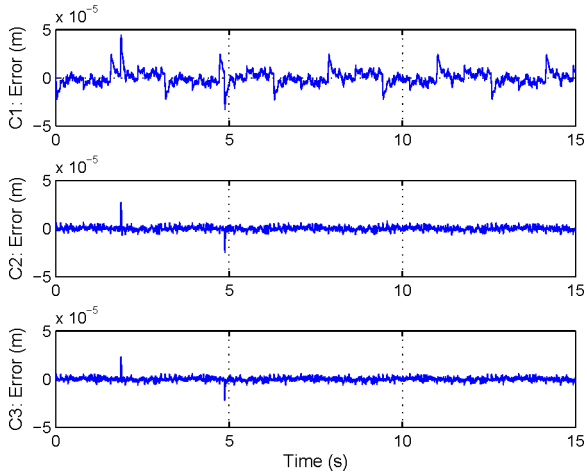

Fig. 6. Circular contouring errors of set 3 (disturbances).

large disturbances do not affect the contouring performance of ARC and DCARC much except the transient spikes when the sudden changes of the disturbances occur—even the transient tracking errors are within 24 μm for DCARC. All these results demonstrate the strong performance robustness of the proposed schemes.

2) Elliptical Contouring With Constant Angular Velocity: To test the contouring performance of the proposed algorithms for noncircular motions, the biaxial gantry is also commanded to track an ellipse described by

$$\mathbf{q_d} = \begin{bmatrix} x_d(t) \\ y_d(t) \end{bmatrix} = \begin{bmatrix} 0.2\sin(3t) \\ -0.1\cos(3t) + 0.1 \end{bmatrix} \tag{40}$$

which has an angular velocity of $\omega = 3$ rad/s.

The elliptical contouring experimental results in terms of performance indexes after running the gantry for one period are given in Table II. The same qualitative comparative performance results as in the circular contouring experiments can be drawn from the table. For set 1, the desired ellipse and the actual contours by all three controllers are shown in Fig. 7, and the contouring errors are displayed in Fig. 8, which are mostly

TABLE II
ELLIPTICAL CONTOURING RESULTS

	$\|\|\varepsilon_c\|\|_{rms}$	ε_{cM}	$\|\|\varepsilon_t\|\|_{rms}$	$\|\|u_x\|\|_{rms}$	$\|\|u_y\|\|_{rms}$
C1 (Set1)	$8.98\mu m$	$24.81\mu m$	$6.60\mu m$	0.30V	0.45V
C2 (Set1)	$2.67\mu m$	$9.55\mu m$	$6.88\mu m$	0.36V	0.49V
C3 (Set1)	$2.14\mu m$	$8.21\mu m$	$5.17\mu m$	0.37V	0.51V
C1 (Set2)	$9.40\mu m$	$26.89\mu m$	$7.48\mu m$	0.36V	0.49V
C2 (Set2)	$2.90\mu m$	$10.62\mu m$	$7.09\mu m$	0.40V	0.52V
C3 (Set2)	$2.35\mu m$	$9.31\mu m$	$5.10\mu m$	0.40V	0.53V
C1 (Set3)	$10.24\mu m$	$43.13\mu m$	$7.12\mu m$	0.30V	0.45V
C2 (Set3)	$3.07\mu m$	$24.56\mu m$	$6.77\mu m$	0.36V	0.49V
C3 (Set3)	$2.50\mu m$	$21.94\mu m$	$5.28\mu m$	0.37V	0.50V

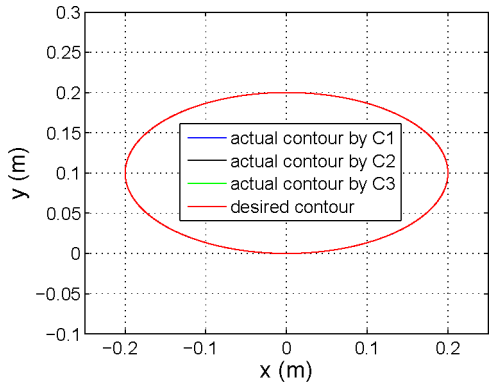

Fig. 7. Elliptical contouring of set 1 in X–Y plane.

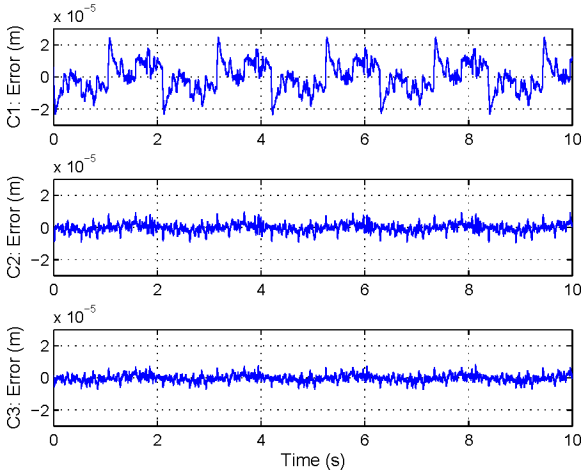

Fig. 8. Elliptical contouring errors of set 1 (no load).

within 5 μm for both ARC and DCARC. For set 2, the contouring errors are shown in Fig. 9, which are almost the same as those without the payload for ARC and DCARC, demonstrating the strong performance robustness of both controllers to the change of inertia load. The contouring errors of set 3 are given in Fig. 10. Again, the added large disturbances do not affect the contouring performance of ARC and DCARC much except the initial transient when the sudden changes of the disturbances occur. All these results further demonstrate the strong performance robustness of the proposed schemes.

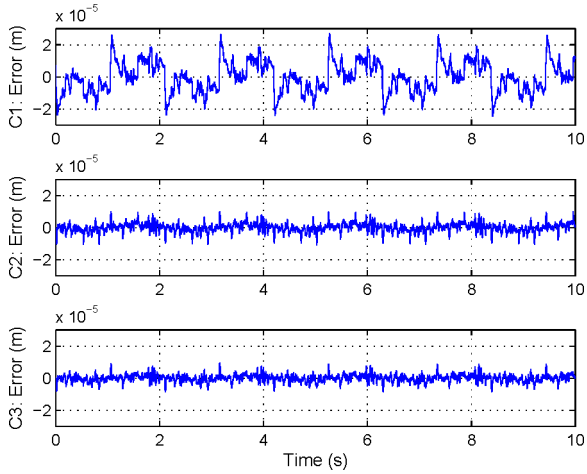

Fig. 9. Elliptical contouring errors of set 2 (loaded).

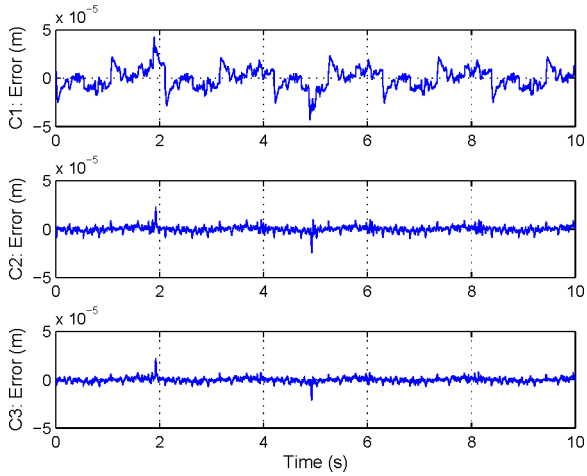

Fig. 10. Elliptical contouring errors of set 3 (disturbances).

VII. CONCLUSION

In this paper, coordinated adaptive robust contouring controllers have been developed for a biaxial linear-motor-driven precision gantry in the presence of both parametric uncertainties and uncertain nonlinearities, including unmodeled cogging forces and external disturbances. It was shown that the proposed controllers theoretically guarantee a prescribed contouring performance, in general, while achieving asymptotic tracking in the presence of parametric uncertainties only. Extensive comparative experimental results for reasonably high-speed circular and elliptical motions have demonstrated the good contouring performance of the proposed coordinated ARC controllers in actual applications and the strong performance robustness of the controllers to parameter variations and disturbances.

REFERENCES

[1] D. M. Alter and T. C. Tsao, "Control of linear motors for machine tool feed drives: Design and implementation of h_∞ optimal feedback control," *Trans. ASME, J. Dyn. Syst., Meas., Control*, vol. 118, pp. 649–656, 1996.

[2] C.-L. Lin, H.-Y. Jan, and N.-C. Shieh, "GA-based multiobjective PID control for a linear brushless DC motor," *IEEE/ASME Trans. Mechatronics*, vol. 8, no. 1, pp. 56–65, Mar. 2003.
[3] Y. Hong and B. Yao, "A globally stable high performance adaptive robust control algorithm with input saturation for precision motion control of linear motor drive system," *IEEE/ASME Trans. Mechatronics*, vol. 12, no. 2, pp. 198–207, Apr. 2007.
[4] L. Lu, Z. Chen, B. Yao, and Q. Wang, "Desired compensation adaptive robust control of a linear motor driven precision industrial gantry with improved cogging force compensation," *IEEE/ASME Trans. Mechatronics*, vol. 13, no. 6, pp. 617–624, Dec. 2008.
[5] Y. Hong and B. Yao, "A globally stable saturated desired compensation adaptive robust control for linear motor systems with comparative experiments," *Automatica*, vol. 43, no. 10, pp. 1840–1848, Oct. 2007.
[6] G. T.-C. Chiu and M. Tomizuka, "Contouring control of machine tool feed drive systems: A task coordinate frame approach," *IEEE Trans. Control Syst. Technol.*, vol. 9, no. 1, pp. 130–139, Jan. 2001.
[7] Y. Li and Q. Xu, "Development and assessment of a novel decoupled XY parallel micropositioning platform," *IEEE/ASME Trans. Mechatronics*, to be published.
[8] S. Bashash and N. Jalili, "Robust adaptive control of coupled parallel piezo-flexural nanopositioning stages," *IEEE/ASME Trans. Mechatronics*, vol. 14, no. 1, pp. 11–20, Feb. 2009.
[9] Y. Koren, "Cross-coupled biaxial computer control for manufacturing systems," *Trans. ASME, J. Dyn. Syst., Meas., Control*, vol. 102, pp. 265–272, 1980.
[10] Y. T. Shih, C. S. Chen, and A. C. Lee, "A novel cross-coupling control design for bi-axis motion," *Int. J. Mach. Tools Manuf.*, vol. 42, pp. 1539–1548, 2002.
[11] S.-S. Yeh and P.-L. Hsu, "Estimation of the contouring error vector for the cross-coupled control design," *IEEE/ASME Trans. Mechatronics*, vol. 7, no. 1, pp. 44–51, Mar. 2002.
[12] K.-H. Su and M.-Y. Cheng, "Contouring accuracy improvement using cross-coupled control and position error compensator," *Int. J. Mach. Tools Manuf.*, vol. 48, pp. 1444–1453, 2008.
[13] M.-Y. Cheng and C.-C. Lee, "Motion controller design for contour-following tasks based on real-time contour error estimation," *IEEE Trans. Ind. Electron.*, vol. 54, no. 3, pp. 1686–1695, Jun. 2007.
[14] C.-L. Chen and K.-C. Lin, "Observer-based contouring controller design of a biaxial stage system subject to friction," *IEEE Trans. Control Syst. Technol.*, vol. 16, no. 2, pp. 322–329, Mar. 2008.
[15] B. Yao, "High performance adaptive robust control of nonlinear systems: A general framework and new schemes," in *Proc. IEEE Conf. Decis. Control*, 1997, pp. 2489–2494.
[16] B. Yao and M. Tomizuka, "Smooth robust adaptive sliding mode control of robot manipulators with guaranteed transient performance," *Trans. ASME, J. Dyn. Syst., Meas., Control*, vol. 118, no. 4, pp. 764–775, 1996.
[17] B. Yao and M. Tomizuka, "Adaptive robust control of SISO nonlinear systems in a semi-strict feedback form," *Automatica*, vol. 33, no. 5, pp. 893–900, 1997.
[18] X. Zhu, G. Tao, B. Yao, and J. Cao, "Adaptive robust posture control of parallel manipulator driven by pneumatic muscles with redundancy," *IEEE/ASME Trans. Mechatronics*, vol. 13, no. 4, pp. 441–450, Aug. 2008.
[19] L. Xu and B. Yao, "Adaptive robust precision motion control of linear motors with negligible electrical dynamics: Theory and experiments," *IEEE/ASME Trans. Mechatronics*, vol. 6, no. 4, pp. 444–452, Dec. 2001.
[20] B. Yao, F. Bu, J. Reedy, and G. T.-C. Chiu, "Adaptive robust control of single-rod hydraulic actuators: Theory and experiments," *IEEE/ASME Trans. Mechatronics*, vol. 5, no. 1, pp. 79–91, Mar. 2000.
[21] B. Yao, M. Al-Majed, and M. Tomizuka, "High performance robust motion control of machine tools: An adaptive robust control approach and comparative experiments," *IEEE/ASME Trans. Mechatronics*, vol. 2, no. 2, pp. 63–76, Jun. 1997.
[22] L. Xu and B. Yao, "Coordinated adaptive robust contour tracking of linear-motor-driven tables in task space," in *Proc. 39th IEEE Conf. Decis. Control*, Dec. 12–15, 2000, vol. 3, pp. 2430–2435.
[23] B. Yao, S. P. Chan, and D. Wang, "Unified formulation of variable structure control schemes to robot manipulators," *IEEE Trans. Autom. Control*, vol. 39, no. 2, pp. 371–376, Feb. 1994.
[24] B. Yao, "Desired compensation adaptive robust control," *Trans. ASME, J. Dyn. Syst., Meas., Control*, to be published.
[25] B. Yao and M. Tomizuka, "Adaptive robust motion and force tracking control of robot manipulators in contact with compliant surfaces with unknown stiffness," *Trans. ASME, J. Dyn. Syst., Meas., Control*, vol. 120, no. 2, pp. 232–240, 1998.
[26] B. Yao and L. Xu, "Adaptive robust control of linear motors for precision manufacturing," *Int. J. Mechatronics*, vol. 12, no. 4, pp. 595–616, 2002.
[27] N. Sadegh and R. Horowitz, "Stability and robustness analysis of a class of adaptive controllers for robot manipulators," *Int. J. Robot. Res.*, vol. 9, no. 3, pp. 74–92, 1990.

Chuxiong Hu (S'09) received the B.Eng degree in 2005 from Zhejiang University, Hangzhou, China, where he is currently working toward the Ph.D. degree in mechatronic control engineering.

His current research interests include coordinated motion control, precision mechatronics, adaptive robust control, and nonlinear systems.

Bin Yao (S'92–M'96–SM'09) received the B.Eng. degree in applied mechanics from Beijing University of Aeronautics and Astronautics, Beijing, China, in 1987, the M.Eng. degree in electrical engineering from Nanyang Technological University, Singapore, in 1992, and the Ph.D. degree in mechanical engineering from the University of California, Berkeley, in 1996.

Since 1996, he has been with the School of Mechanical Engineering, Purdue University, West Lafayette, IN, where he became a Professor in 2007. He is also with Zhejiang University, Hangzhou, China, where he was honored as the Kuang-piu Professor in 2005. Since 2006, he has been an Associate Editor of the *Journal of Dynamic Systems, Measurement, and Control*.

Prof. Yao was awarded a Faculty Early Career Development (CAREER) Award from the National Science Foundation in 1998 and a Joint Research Fund for Outstanding Overseas Chinese Young Scholars from the National Natural Science Foundation of China in 2005. He was also the recipient of the O. Hugo Schuck Best Paper (Theory) Award from the American Automatic Control Council in 2004 and the Outstanding Young Investigator Award of the ASME Dynamic Systems and Control Division (DSCD) in 2007. He has chaired numerous sessions and has been a member of the international program committees of various IEEE, ASME, and International Federation of Automatic Control conferences. From 2000 to 2002, he was the Chair of the Adaptive and Optimal Control Panel, and from 2001 to 2003, the Chair of the Fluid Control Panel of the ASME DSCD. He is currently the Vice Chair of the ASME DSCD Mechatronics Technical Committee. He was a Technical Editor of the IEEE/ASME TRANSACTIONS ON MECHATRONICS from 2001 to 2005. He is a member of the ASME.

Qingfeng Wang received the M.Eng. and Ph.D. degrees in mechanical engineering from Zhejiang University, Hangzhou, China, in 1988 and 1994, respectively.

He was a faculty member at Zhejiang University, where he became a Professor in 1999, was the Director of the State Key Laboratory of Fluid Power Transmission and Control from 2001 to 2005, and is currently the Director of the Institute of Mechatronic Control Engineering. His research interests include electrohydraulic control components and systems, hybrid power systems and energy saving techniques for construction machinery, and system synthesis for mechatronic equipment.